



The surface chemistry of norbornadiene and norbornene on Pd(111) and Pd(100): a comparative DFT study

Ravshan S. Shamsiev¹

Received: 24 August 2023 / Accepted: 27 September 2023 / Published online: 16 October 2023
© The Author(s), under exclusive licence to Springer-Verlag GmbH Germany, part of Springer Nature 2023

Abstract

Context The interaction of norbornadiene (NBD) and norbornene (NBE) with the palladium (111) and (100) surfaces have been investigated using density functional theory (DFT). Five configurations of adsorbed NBD may be formed on Pd(111): *endo*-tetra- σ , *endo*-di- σ,π , *endo*-di- π , *exo*-di- σ , and *exo*- π . The NBE molecule adsorbed on Pd(111) may exist in 4 configurations: *endo*-di- σ , *endo*- π , *exo*-di- σ , and *exo*- π . On Pd(100), a smaller number adsorption configurations of NBD and NBE are formed, since the double bonds of these molecules in the *endo*-orientation are bound only in a di- σ mode. The adsorption energy of NBD and NBE molecules on Pd(100) is noticeably higher compared to Pd(111), which is due to the surface geometry of Pd(100). The most stable configurations on both Pd facets are *endo*-tetra- σ for NBD and *exo*-di- σ for NBE. However, due to smaller adsorption area of the *exo*-di- σ configuration on Pd(111), a larger number of NBD molecules may adsorbed on the same surface area. Energetically favorable *endo*-tetra- σ (NBD) and *exo*-di- σ (NBE) configurations are very mobile on Pd(111). On Pd(100), only NBE molecules can migrate, while NBD migration is hindered due to the high activation barrier. **Methods** All DFT calculations were performed using the Perdew-Burke-Ernzerhof density functional (PBE) with the relativistic SBK effective core potential and TZ2P basis set in the PRIRODA program.

Keywords Adsorption · Palladium · Norbornadiene · Norbornene · Strained hydrocarbons

Introduction

Norbornadiene (bicyclo[2.2.1]hepta-2,5-diene, NBD), norbornene (bicyclo[2.2.1]hept-2-ene, NBE) and their derivatives have attracted the attention of researchers for many years [1, 2]. These compounds are widely used in the production of polymers with desired properties [3–8] and pharmaceuticals [9–12], in the perfumery industry [13, 14] and microelectronics [15, 16], and also as solar energy converters [17–21]. The use of NBD and NBE is not limited to the role of prospective semiproducts for organic syntheses. In the Catellani reaction, i.e. Pd-catalyzed C–H functionalization of arenes, NBE is actually a co-catalyst for the synthesis of polyfunctionalized arenes [22–24].

The NBD molecule has two double bonds and C_{2v} symmetry, while NBE has one double bond and C_s symmetry

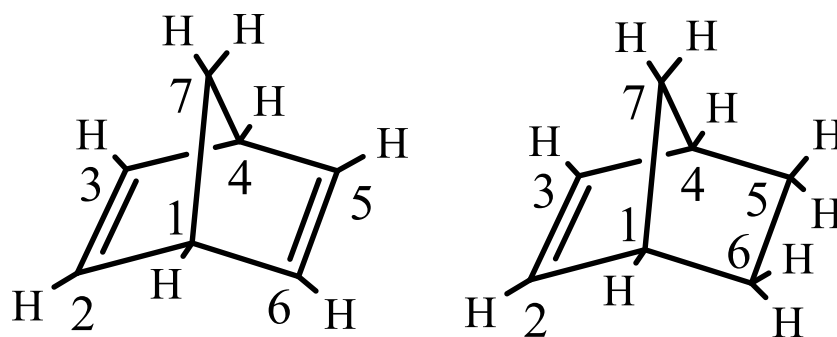
(Fig. 1). The presence of a methylene (C7) bridge leads to a significant strain in both molecules (ring strain energies = 32.3 (NBD) and 21.6 (NBE) kcal/mol [25]). In particular, the bond angles C1C7C4, C2C1C6, and C2C1C7 are much smaller [26, 27] than the tetrahedral angle. Due to the high ring strain the double bonds of NBD and NBE have an increased reactivity. Unlike conjugated dienes, the double bonds in the NBD molecule are separated by a CH₂ group. However, recent works [28] show that NBE does not enter into the hydrogenation reaction in the presence of NBD. The development of new selective catalysts and the selection of the conditions for carrying out the partial hydrogenation of unsaturated compounds are fundamental tasks of catalysis. In addition, the hydrogenation of one of the two double bonds of cyclic dienes is of interest for the subsequent synthesis of their functional derivatives. Pd-based catalysts are among the most active and selective in the partial hydrogenation of alkynes and dienes [29–35].

It is known from the literature that the selective hydrogenation of one double bond is also possible in cyclo-dienes with non-conjugated double bonds, for example, the hydrogenation of 1,4-cyclohexadiene [36, 37] and 1,5-cyclooctadiene

✉ Ravshan S. Shamsiev
shamsiev.r@gmail.com

¹ MIREA – Russian Technological University, Lomonosov
Institute of Fine Chemical Technologies, 86 Vernadsky
Avenue, 119571 Moscow, Russian Federation

Fig. 1 Carbon atom numbering and structures of NBD and NBE molecules



[33–35]. The sequential nature of the hydrogenation of double bonds is possible if the hydrogenation rates of the first and second double bonds are noticeably different. Under the conditions of heterogeneous catalysis, an important role is played by the selective adsorption of the diene on the active site [36]. The selectivity depends on the relative adsorption strength, configuration of substrates and the structure of active sites [38]. Thus, the study of adsorption of unsaturated substrates on a metal surface is extremely important for understanding the mechanisms of reactions involving them and, in particular, the hydrogenation. Detailed information about the ways by which the substrate molecules interact with the catalyst surface can be obtained using quantum chemical modeling.

On the basis of UV-photoelectron spectroscopy (UPS), high-resolution X-ray photoelectron spectroscopy (XPS), and near edge X-ray absorption fine structure (NEXAFS) in combination with DFT calculations it was shown [39] that during NBD adsorption, the double bonds are parallel to the Ni(111) surface and form an $\eta^2:\eta^2$ adsorption configuration (Fig. 2a) with an adsorption energy of 54.0 kcal/mol. The presence of CN groups at the C2 and C3 atoms of the NBD molecule does not interfere with the interaction of the disubstituted double bond with the Ni(111) surface [40]. The adsorption energy of the NBD molecule in the $\eta^2:\eta^1$ configuration with the agostic C-H bond [39] of the CH_2 -bridge group (Fig. 2b) is significantly lower (38.5 kcal/mol). Similar adsorption structures of the NBD molecule were identified on the Pt(111) surface [41, 42], corresponding to two

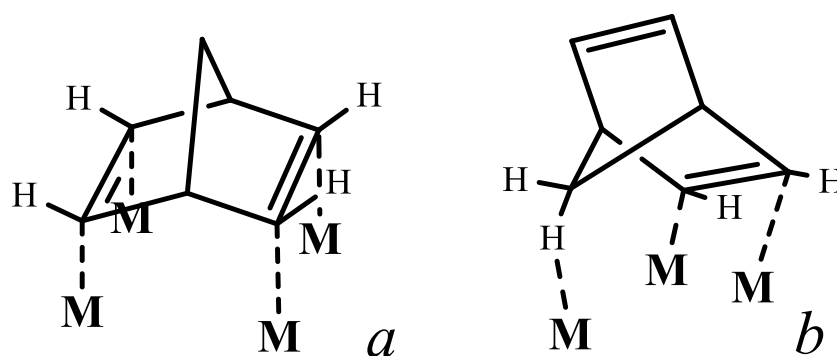
configurations $\eta^2:\eta^2$ and $\eta^2:\eta^1$. The corresponding adsorption energies are noticeably higher (~83 and 56 kcal/mol) as compared to the Ni(111) surface. Chemisorption of NBD is also possible on non-metallic surfaces. For example, the adsorption energy of the NBD molecule on the Si(001) surface varies within 72–96 kcal/mol [43]. There are significantly fewer works in the literature related to the study of NBE adsorption as compared to NBD. According to DFT calculations [44], the adsorption energy of NBE on the Ge(100) surface is 24.4 kcal/mol.

The main goal of this work was a DFT study of the structure and energy of possible adsorption configurations of NBD and NBE molecules on Pd(111) and Pd(100) surfaces.

Computational methods and models

The quantum chemical calculations were performed using the PRIRODA computer code [45, 46]. The generalized-gradient approximation of density functional theory (DFT) with the Perdew-Burke-Ernzerhof exchange–correlation functional (PBE) [47] was used. Relativistic effects were considered using the SBK effective core potential [48] with TZ2P basis set (Table S1). The use of effective core potential makes it possible to noticeably reduce computational costs, while the accuracy decreases insignificantly. Previously, it was shown that PBE/SBK calculated binding energies in Pd_2 and PdH molecules are in good agreement with the all-electron scalar-relativistic calculations [49]. In this work,

Fig. 2 NBD $\eta^2:\eta^2$ (a) and $\eta^2:\eta^1$ (b) adsorption configurations on Ni(111) [39] and Pt(111) surfaces [41, 42]



to verify the adequacy of the PBE/SBK method, we calculated the adsorption of an ethylene molecule in the di- σ configuration on the surface of a Pd₃₉ particle. The atomic structure of the Pd₃₉ surface corresponds to the (111) facet (Figure S1). For comparison, calculations were performed in the all-electron scalar-relativistic approximation of DFT-PBE and the L22m basis set [50, 51], as well as in the PBE0 hybrid functional with 25% Hartree–Fock exchange energy [52]. The calculation results are presented in Table 1.

Table 1 shows that the PBE/SBK calculated adsorption energy E_{ads} of C₂H₄ (24.6 kcal/mol) agrees well with the all-electron PBE/L22m calculations (24.0 kcal/mol). According to the PBE0/SBK calculations, the $E_{\text{ads}}(\text{C}_2\text{H}_4)$ value is slightly higher than in the PBE/SBK calculations (by 4.1 kcal/mol). The periodic DFT-PW91 calculations [53–55] of $E_{\text{ads}}(\text{C}_2\text{H}_4)$ and the geometric parameters of the di- σ configuration are also in good agreement with our PBE/SBK calculations. It should be noted that the computational costs of the PBE/L22m and PBE0/SBK methods are much higher. In addition, convergence problems arise with an increase of the number of Pd atoms.

In our study of the adsorption of NBD and NBE, a Pd₈₆ nanoparticle with (111) and (100) facets, obtained by truncating an octahedral Pd₁₄₀ cluster, was used as a model of the palladium surface. The optimized structure of Pd₈₆ is shown in Fig. 3. Previously, this model was used to study the adsorption of phenylacetylene and styrene on the Pd surface [56]. Table 2 illustrates the values

Table 1 Adsorption energy (E_{ads}) of C₂H₄ on Pd₃₉, C=C and C–Pd bond distances for di- σ configuration

Method	$R_{\text{C=C}}$ Å	$R_{\text{C-Pd}}$	E_{ads} kcal/mol
PBE/SBK	1.45	2.13	24.6
PBE/L22m	1.45	2.11	24.0
PBE0/SBK	1.45	2.06	28.7
PW91	1.45 ^{a,b}	2.12 ^{a,b}	21.5 ^a , 22.5 ^b , 19.6 ^c

^aref. [53], ^bref. [54], ^cref. [55]

Fig. 3 Side view of the (100) and (111) facets of the Pd₈₆ cluster

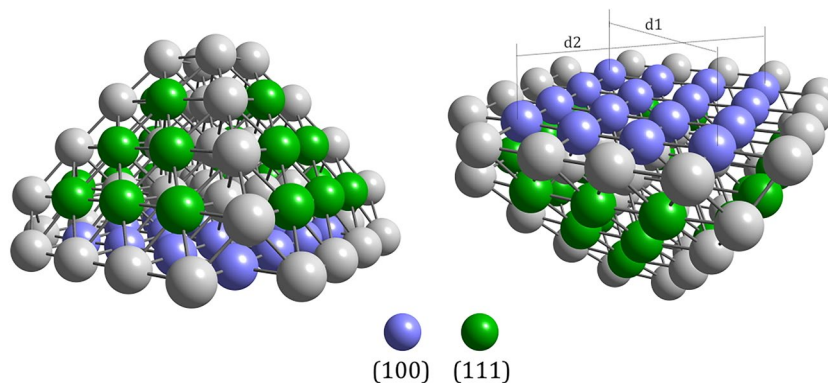


Table 2 Calculated properties of Pd₈₆ in various spin multiplicities (2S + 1): relative energy (ΔE), Pd–Pd bond distances (min–max) on the (111) and (100) facets, d_1 and d_2 diagonals of the (100) facet

2S + 1	ΔE kcal/mol	R_{111} Å	R_{100}	d_1, d_2
1	0.0	2.70–2.72	2.64–2.71	11.18, 11.24
3	-4.1*	2.70–2.73	2.63–2.74	11.07, 11.31
5	-4.1*	2.70–2.72	2.63–2.74	10.94, 11.45

*from ref. [56]

of the relative energies of Pd₈₆ in various electronic states and the ranges of the Pd–Pd bond lengths R_{111} and R_{100} for the (111) and (100) facets, respectively. The triplet and quintet spin states of Pd₈₆ have lower energies [56]. However, geometry optimization of these states leads to structural deformation of Pd₈₆, which manifests itself in the elongation of one diagonal on the (100) facet and the shortening of the other (d_1 and d_2 , Fig. 3). As can be seen from the last column of Table 2, the diagonals d_1 and d_2 are markedly different. In turn, the asymmetry of the d_1 and d_2 diagonals leads to a distortion of the shape of the (111) and (100) faces. The deformation of Pd₈₆ increases with increasing multiplicity. Adsorption of NBD or NBE molecules also enhances the deformation of the Pd₈₆ particle. To exclude a noticeable symmetry breaking, the singlet state for Pd₈₆ was taken in further calculations.

The adsorption energy of NBD and NBE molecules on the palladium surface was calculated by the relation:

$$E_{\text{ads}} = -[E(\text{molecule/Pd}_{86}) - E(\text{molecule}) - E(\text{Pd}_{86})] \quad (1)$$

where $E(\text{molecule/Pd}_{86})$, $E(\text{molecule})$, and $E(\text{Pd}_{86})$ are the total energies of the Pd₈₆ cluster with the adsorbed NBD/NBE molecule, the Pd₈₆ cluster, and the free NBD/NBE molecule, respectively. In this work, to calculate the adsorption energy, Eq. (1) was chosen, which coincides in sign with the binding energy and is opposite in sign with the

adsorption enthalpy to eliminate confusion when discussing the relative stability of adsorption configurations. Vibrational frequency analysis of the optimized adsorption structures was utilized to ensure that it was true local minimum having no imaginary frequencies. The adsorption energy including zero-point vibrational energy (ZPVE) corrections is designated as $E_{\text{ads},0}$.

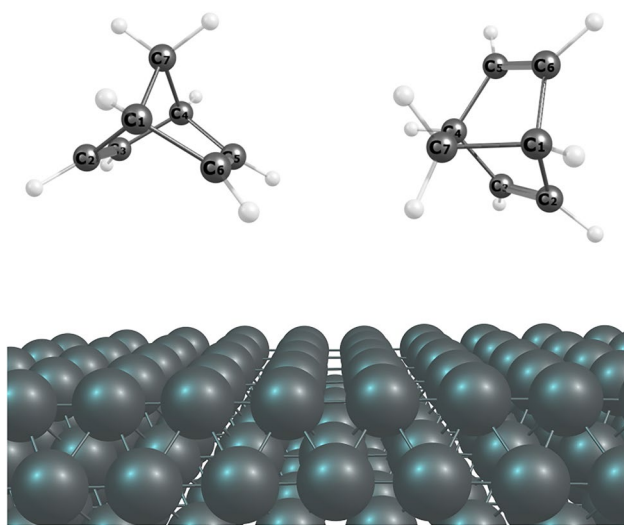


Fig. 4 *Endo-* (left) and *exo-* (right) orientation of NBD relative to a surface

Results and discussion

Based on the data on the adsorption of NBD and NBE molecules on Ni and Pt surfaces [39, 41, 42], it can be concluded that the interaction of these molecules with metal atoms is in many respects similar to the *endo/exo* coordination of the double bond of these molecules on one metal atom [41]. In the same way, when approaching the surface, NBD and NBE molecules can have an *endo*-orientation if the surface atoms and the CH₂-bridge group are on opposite sides of the plane of the adsorbed double bond (C2C3C5C6), and an *exo*-orientation if the surface atoms are on the same side with the CH₂-bridge group (Fig. 4). According to our calculations, NBD and NBE molecules are adsorbed on the Pd surface in several possible ways and are not limited to two configurations (Fig. 2) described for other metals [39–44].

Adsorption of NBD and NBE molecules on Pd(111)

For the NBD molecule, the type of adsorption configuration formed depends, first of all, on its *endo/exo* orientation when approaching the surface. In the case of *endo*-orientation, both double bonds of the NBD molecule interact with surface Pd atoms, resulting in the formation of 3 adsorption configurations, **tetra- σ** , **di- σ,π** , and **di- π** . The **tetra- σ** configuration corresponds to the $\eta^2:\eta^2$ configuration (Fig. 2a). Optimized structures are shown in Fig. 5. Calculated adsorption energies, C=C

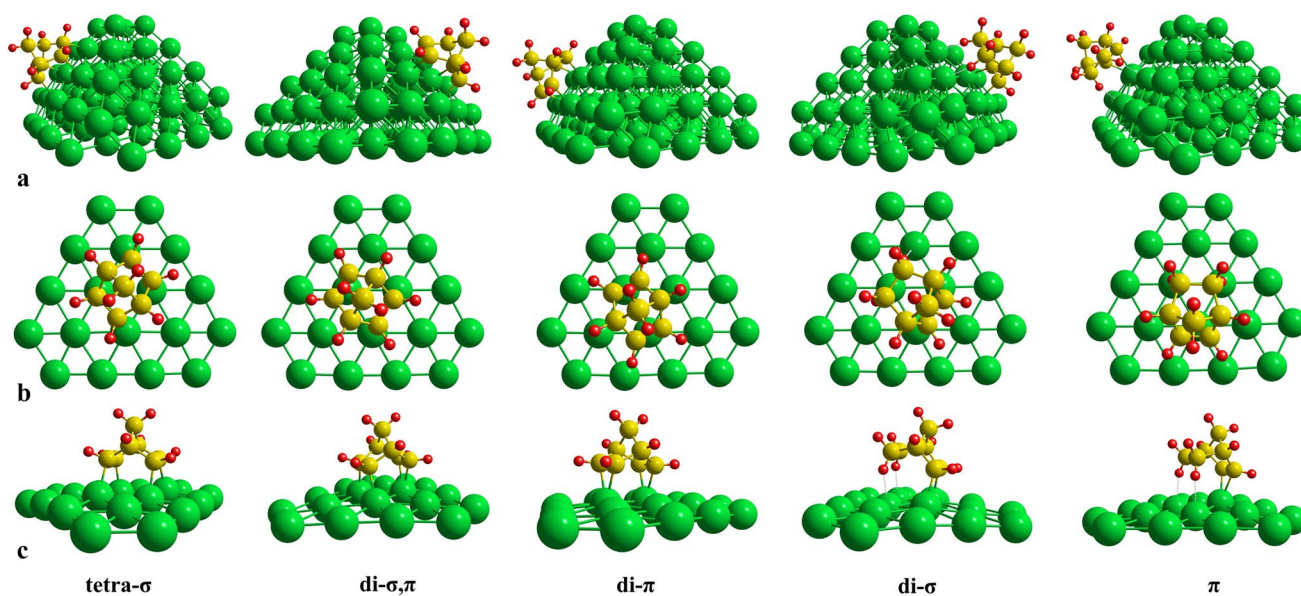
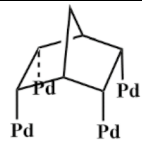
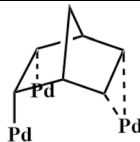
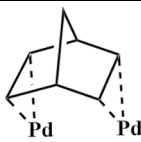
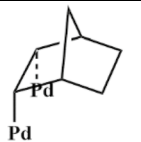
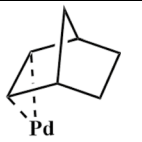


Fig. 5 Optimized structures of NBD (**tetra- σ** , **di- σ,π** , and **di- π**) and NBE (**di- σ** and **π**) *endo*-adsorption configurations on Pd(111): *a* – side views of Pd₈₆, *b* – top views of NBD/NBE (the first layer of the

Pd atoms are shown), *c* – side views of the C1(4) atom of NBD/NBE molecule (the first layer of the Pd atoms are shown)

Table 3 Adsorption energies (E_{ads} and $E_{\text{ads},0}$, kcal/mol), C=C and C–Pd bond lengths ($R_{\text{C}=\text{C}}$ and $R_{\text{C}-\text{Pd}}$, Å), C2C1C7 bond angle (deg.) of *endo*-adsorption configurations of NBD and NBE on Pd(111)

Parameter	NBD			NBE	
	 tetra- σ	 di- σ, π	 di- π	 di- σ	 π
E_{ads}	43.7	37.8	25.9	18.1	9.5
$E_{\text{ads},0}$	43.2	37.3	25.6	18.3	10.1
$R_{\text{C}=\text{C}}$	1.482, 1.484 ^a	1.490, 1.420 ^a 1.34 ^b	1.420, 1.425 ^a	1.489	1.417
$R_{\text{C}-\text{Pd}}^c$	2.079–2.127	2.084–2.214	2.146–2.218	2.109–2.115	2.213–2.244
C2C1C7	99.0	98.6	97.5	98.2	97.8

^aC5C6 bond length of NBD; ^bC2C3 bond length of free NBD/NBE; ^crange of C–Pd bond lengths.

and C–Pd bond lengths, and C2C1C7 bond angle are presented in Table 3.

In the **tetra- σ** , **di- σ, π** , and **di- π** configurations the carbon atoms of NBD are bonded with 4, 3, and 2 Pd atoms, respectively. The adsorption energy of the NBD molecule on Pd(111) decreases in the same order. The strongest is the **tetra- σ** configuration, in which both NBD double bonds are di- σ -adsorbed. The energy of interaction of the di- σ -adsorbed double bond with Pd atoms is approximately equal to half of E_{ads} (**tetra- σ**), i.e., 21.85 kcal/mol, which is slightly less than the adsorption energy of ethylene (24.6 kcal/mol, Table 1). The length of the NBD double bond in the **tetra- σ** configuration is markedly increased (1.48 Å). This distance is closer to the single bond of the norbornane molecule than to the double bond of the NBD molecule. For comparison, the C2C3 bond lengths in free NBD and norbornane (C₇H₁₂) molecules are 1.34 Å [26, 57] and 1.57 Å [58], respectively.

Both double bonds are π -adsorbed in the **di- π** configuration. This mode of interaction with Pd atoms activates the double bond less, so the length of the double bond (1.42 Å) is longer than in the case of the **tetra- σ** configuration. The binding energy of each π -adsorbed double bond with a Pd atom is approximately equal to 12.95 kcal/mol.

The threefold site of Pd(111) stabilizes an intermediate **di- σ, π** configuration in which one double bond is di- σ -adsorbed and the other is π -adsorbed. The lengths of NBD double bonds in the **di- σ, π** configuration are 1.49 Å and 1.42 Å, respectively, and correspond to the **tetra- σ** and **di- π** configurations (Table 3).

The NBE molecule has only one double bond, which forms with Pd(111) two possible configurations upon

endo-adsorption, **di- σ** and **π** . The lengths of the adsorbed double bonds of NBE and NBD molecules are close, but in the case of NBE, the binding energy of the double bond with Pd atoms is noticeably lower, 18.1 and 9.5 kcal/mol for di- σ - and π -adsorbed double bonds (Table 3). For comparison, in the NBD molecule these energies are 21.85 and 12.95 kcal/mol. The additional energy gain during NBD adsorption is associated with the prevalence of ring strain energy of the NBD molecule. Thus, the C2C1C7 bond angle for the NBD **tetra- σ** configuration is larger than for the NBE **di- σ** configuration (99.0° and 98.2°, Table 3). According to experimental data, this angle in free NBD and norbornane molecules is 98.4° [59] and 102.0° [58], respectively. Two hydrogen atoms in the *endo*-**di- σ** and *endo*- **π** configurations of NBE interact with surface Pd atoms. In the case of *endo*-**di- σ** configuration each H atom is not above one Pd atom, but between two (**di- σ** , Fig. 5) due to the triangular geometry of the threefold sites of Pd(111). As a result, the H–Pd interaction is not strong, and the shortest H–Pd distances are 2.38 and 2.54 Å.

The *exo*-approach of NBD and NBE molecules to Pd(111) leads to the formation of **di- σ** and **π** configurations, in which only one double bond interacts with two (for **di- σ**) or one (for **π**) Pd atoms. The *exo*-**di- σ** configuration corresponds to the $\eta^2:\eta^1$ configuration (Fig. 2b). Optimized structures are shown in Fig. 6. Calculated adsorption energies, C2=C3 and C–Pd bond lengths, and C2C1C7 bond angle are presented in Table 4. The adsorption energy of NBD in the *exo*-**di- σ** and *exo*- **π** configurations is 6.4–6.9 kcal/mol higher than the adsorption energy in the *endo*-**tetra- σ** and *endo*-**di- π** configurations

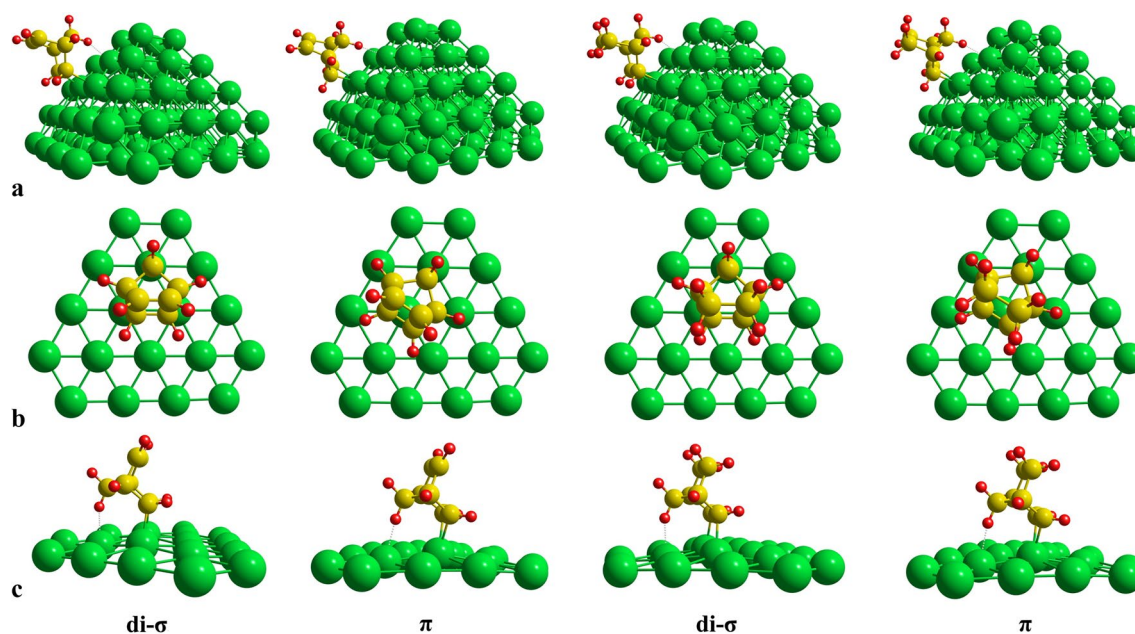
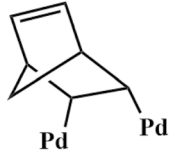

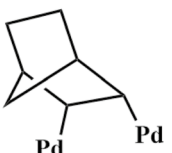



Fig. 6 Optimized structures of *exo*-adsorption configurations of NBD and NBE on Pd(111): *a* – side views of Pd₈₆, *b* – top views of NBD/NBE (the first layer of the Pd atoms are shown), *c* – side views of the C1(4) atom of NBD/NBE molecule (the first layer of the Pd atoms are shown)

Table 4 Adsorption energies (E_{ads} and $E_{\text{ads},0}$, kcal/mol), C2=C3 and C–Pd bond lengths ($R_{\text{C}2\text{C}3}$ and $R_{\text{C-Pd}}$, Å), C2C1C7 bond angle (deg.) of *exo*-adsorption configurations of NBD and NBE on Pd(111)

Parameter	NBD		NBE	
	 Pd Pd di- σ	 Pd π	 Pd Pd di- σ	 Pd π
E_{ads}	28.7	19.4	25.8	18.9
$E_{\text{ads},0}$	28.5	19.2	25.7	18.8
$R_{\text{C}2\text{C}3}$	1.490	1.422	1.480	1.420
$R_{\text{C-Pd}}$	2.106, 2.108	2.195, 2.198	2.121, 2.122	2.211, 2.216
C2C1C7	102.0	101.5	103.0	102.7

^aC5C6 bond length of NBD; ^brange of C–Pd bond lengths.

(per one double bond). The main contribution to this difference is made by the interaction energy of the H atom of the methylene bridge with the Pd atom. The distance between metal and hydrogen in the *exo*-**di- σ** and *exo*- **π** configurations is 2.11–2.18 Å, and the C–H–Pd angle is 155.7° and 170.9°, respectively. These geometrical values of the H–Pd interaction do not allow us to attribute it to the agostic type, and it is closer to the anagostic one [60].

Similarly to NBD, in the *exo*-**di- σ** and *exo*- **π** configurations of NBE, there is an anagostic H–Pd interaction. From the energy difference between **di- σ** and **π** configurations in the *exo*- and *endo*-orientation of the NBE molecule, one can approximately estimate the energy of the H–Pd interaction:

$$E_{\text{ads}}(\textit{exo} - \mathbf{di}\text{-}\sigma) - E_{\text{ads}}(\textit{endo} - \mathbf{di}\text{-}\sigma) = 7.7 \text{ kcal/mol}$$

$$E_{\text{ads}}(\textit{exo} - \boldsymbol{\pi}) - E_{\text{ads}}(\textit{endo} - \boldsymbol{\pi}) = 9.5 \text{ kcal/mol}$$

These values are slightly bigger than for NBD (6.4–6.9 kcal/mol). The point is that part of this energy is related not to the H–Pd interaction, but to the fact that the *exo*-configurations of the adsorbed NBE molecule are less strain than the *endo*-configurations. This is indicated by increased C2C1C7 angles (103° and 102.7°, Table 4).

From a comparison of the adsorption energies of NBD and NBE molecules on the (111) facet (Tables 3 and 4), it follows that for NBD, *endo*-adsorption with the formation of the **tetra-σ** configuration is extremely preferable, and for NBE, *exo*-adsorption with the formation of **di-σ** configuration.

Adsorption of NBD and NBE molecules on Pd(100)

The adsorption energies and the main geometrical parameters of the adsorption configurations of NBD and NBE on the (100) facet are given in Table 5. Optimized structures are shown in Fig. 7. We failed to detect the **di-σ,π** and **di-π** configurations of the *endo*-adsorbed NBD molecule on Pd(100). During the geometry optimization these configurations transform into the only possible **tetra-σ** configuration without an activation barrier. In the case of NBE, the *endo*-adsorption leads to the formation of the **di-σ** configuration.

As can be seen from Table 5, the interaction of NBD and NBE with Pd(100) is stronger. The energy gain ΔE_{ads} is especially noticeable for the *endo*-**tetra-σ** configuration of NBD (4.8 kcal/mol). This can be explained by the fact that the fourfold sites of the (100) facet are geometrically better suited for the adsorption of the NBD molecule than the threefold sites of Pd(111).

As in the case of Pd(111), the *exo*-adsorbed NBD and NBE molecules on Pd(100) may exist in two possible configurations, **di-σ** and **π**. The structures of these configurations on the (100) and (111) facets are very close, but the adsorption energies on the (100) facet are higher, especially for the **π** configurations of NBD and NBE ($\Delta E_{\text{ads}} = 3.7\text{--}3.8$ kcal/mol, Table 5). A possible explanation is that the surface atoms of Pd(100) are coordinatively more accessible.

Comparison of E_{ads} for different configurations of NBD and NBE (Table 5) leads to the conclusion that the most energetically favorable configurations on the (100) facet are *endo*-**tetra-σ** (NBD) and *exo*-**di-σ** (NBE) configurations. This means that on Pd(100) the NBD molecule is adsorbed in the *endo*-orientation, while the NBE molecule is adsorbed in the *exo*-orientation. This conclusion is valid for the two considered facets. The adsorption process proceeds without an activation barrier, as evidenced by the energy profiles of NBD desorption from the (100) and (111) facets (Figure S2).

According to [61] the adsorption energy can be decomposed into 3 components: the stabilizing interaction energy (E_{int}) between a molecule and a surface and the destabilizing distortion energy of molecule ($E_{\text{dis,mol}}$) and surface ($E_{\text{dis,Pd}}$):

$$E_{\text{ads}} = E_{\text{int}} - (E_{\text{dis,mol}} + E_{\text{dis,Pd}})$$

Such a decomposition of the adsorption energy for all configurations is presented in Table 6. The distortion energy $E_{\text{dis,mol}}$ calculated as difference between the energies of an isolated molecule in relaxed and in adsorbed geometries; the distortion energy $E_{\text{dis,Pd}}$ calculated as difference between the energies of a surface in relaxed and substrate geometries; and the interaction energy E_{int} calculated as difference between the sum of energies of an isolated molecule in adsorbed geometry and a surface in substrate geometry and the energy of a surface with an adsorbed molecule. As can be seen from Table 6, a strong interaction of NBD and NBE molecules with the Pd surface (31.1–113.4 kcal/mol) compensated by a larger deformation of NBD and NBE molecules (8.7–64.0 kcal/mol).

There are no experimental data on the adsorption of NBD on the palladium surface, however, experiments on the NBD adsorption [41, 42] and the hydrogenation of NBD with dideuterium on Pt(111) [62] indicate the presence of the *exo*-**di-σ** configuration, but not the *endo*-**tetra-σ** configuration. A specific feature of the adsorption of phenylacetylene and styrene on the Pd surface was noted earlier [56]. These molecules interact with the metal

Table 5 Calculated C2=C3 and C–Pd bond lengths (R_{C2C3} and $R_{\text{C–Pd}}$, Å), C2C1C7 bond angle (deg.), adsorption energy (E_{ads} and $E_{\text{ads,0}}$, kcal/mol) and energy gain (ΔE_{ads} , kcal/mol) of adsorption configurations of NBD and NBE on Pd(100)

Configuration	R_{C2C3}	$R_{\text{C–Pd}}^a$	C2C1C7	E_{ads}	$E_{\text{ads,0}}$	ΔE_{ads}^b
NBD						
<i>endo</i> -tetra-σ	1.471, 1.471 ^c	2.099–2.102	111.2	48.4	48.5	4.8
<i>exo</i> -di-σ	1.475	2.112	101.3	29.6	29.7	0.9
<i>exo</i> -π	1.417	2.211, 2.222	101.2	23.0	22.9	3.7
NBE						
<i>endo</i> -di-σ	1.472	2.118	98.6	20.8	21.6	2.7
<i>exo</i> -di-σ	1.464	2.132	102.5	27.3	27.4	1.5
<i>exo</i> -π	1.416	2.227, 2.239	102.5	22.7	22.5	3.8

^arange of C–Pd bond lengths; ^bdefined as the difference between E_{ads} of identical configurations on Pd(100) and Pd(111); ^cC5C6 bond length of NBD

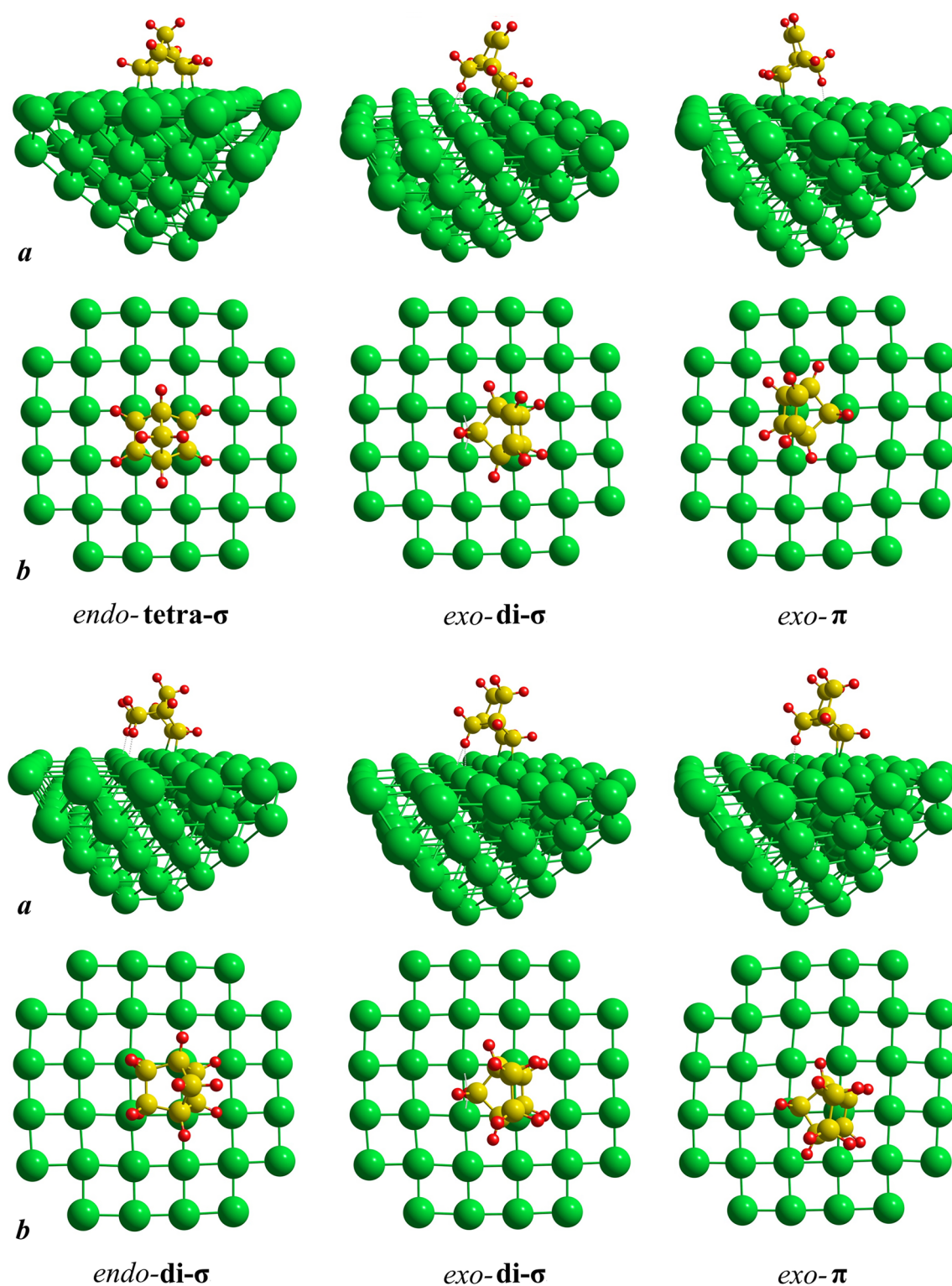


Fig. 7 Optimized structures of adsorption configurations of NBD (upper structures) and NBE (lower structures) on Pd(100): **a** – side view of C1(4) atom of the NBD/NBE molecule, **b** – top view of the NBD/NBE molecule (the first layer of the Pd atoms are shown)

not only with the ethynyl or vinyl group, but also with the aromatic ring. In this case, very strong $\text{di-}\mu_{\text{CC}} + \pi_{\text{Ar}}$ configuration are formed, the hydrogenation rate of which is

much lower [63, 64] than configurations in which the ring is tilted to the Pd surface. DFT calculations [56] showed that adsorption of two phenylacetylene molecules in the

Table 6 Calculated interaction energy (E_{int} , kcal/mol) and distortion energies of NBD and NBE molecules ($E_{\text{dis,mol}}$, kcal/mol) and Pd surface ($E_{\text{dis,Pd}}$, kcal/mol) for all adsorption configurations

Surface	Configuration	E_{int}	$E_{\text{dis,mol}}$	$E_{\text{dis,Pd}}$
Pd(111)				
NBD	<i>endo-tetra-σ</i>	113.4	64.0	5.8
	<i>endo-di-σ,π</i>	87.0	46.1	3.1
	<i>endo-π</i>	60.5	30.4	4.3
	<i>exo-di-σ</i>	62.2	30.0	3.5
	<i>exo-π</i>	35.5	12.4	3.8
NBE	<i>endo-di-σ</i>	60.5	38.3	4.1
	<i>endo-π</i>	30.3	16.2	4.6
	<i>exo-di-σ</i>	52.1	22.8	3.5
	<i>exo-π</i>	31.1	8.7	3.5
Pd(100)				
NBD	<i>endo-tetra-σ</i>	112.3	58.0	5.9
	<i>exo-di-σ</i>	59.8	25.6	4.6
	<i>exo-π</i>	36.2	10.9	2.3
NBE	<i>endo-di-σ</i>	59.8	33.9	5.1
	<i>exo-di-σ</i>	50.9	19.1	4.5
	<i>exo-π</i>	33.5	7.7	3.1

di-μ_{CC} configuration on the same number of Pd atoms is energetically more preferable than one molecule in the **di-μ_{CC} + π_{Ar}** configuration.

It is also possible that in the case of NBD, the experimentally observed *exo-di-σ* configuration on Pt(111) is preferable due to more compact adsorption. Figures 5b and 6b show that the *endo-tetra-σ* configuration occupies 2 sites with a common side, while the *exo-di-σ* configuration occupies 1 threefold site. The binding energy per one Pd atom is:

$$E_{\text{ads}}(\text{endo-tetra-}\sigma)/4 = 10.9 \text{ kcal/mol}$$

$$E_{\text{ads}}(\text{exo-di-}\sigma)/3 = 9.6 \text{ kcal/mol}$$

These values are close, but still the *endo-tetra-σ* configuration according to the binding energy (per Pd atom) remains more preferable.

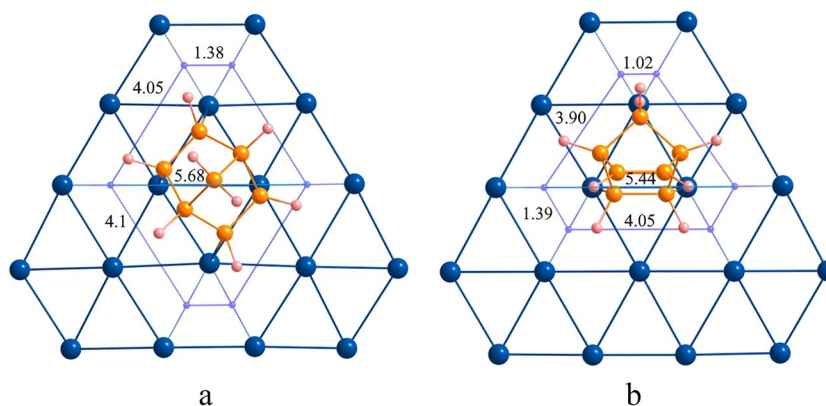
The approximate area of adsorption of one NBD molecule in the *endo-tetra-σ* and *exo-di-σ* configurations is shown in Fig. 8. It can be seen from the figure that the direction of the second double bond away from the Pd surface leads to a significantly smaller area of the *exo*-adsorbed NBD molecule (Fig. 8b), which in turn leads to less steric hindrance for neighboring adsorbed NBD molecules. A simple calculation of the area of these shapes gives the values of 24.4 Å² (S_a) and 16.1 Å² (S_b) for the *endo-tetra-σ* and *exo-di-σ* configurations, respectively, and amounts to 7.6 and 5 areas of threefold site. The ratio $S_a/S_b \approx 1.5$ is approximately the same as the ratio of the $E_{\text{ads}}(\text{endo-tetra-}\sigma)$ and $E_{\text{ads}}(\text{exo-di-}\sigma)$ values. Thus, more compact NBD adsorption in the *exo-di-σ* configuration can compensate for the difference in the adsorption energy $\Delta E_{\text{ads}}(\text{endo-tetra-}\sigma/\text{exo-di-}\sigma)$ due to the interaction of a larger number of NBD with the Pd(111) surface. An example of a compact arrangement of several NBD molecules on Pd(111) is shown in Figure S3.

The feature of the (100) facet leads to the fact that the *endo-tetra-σ* and *exo-di-σ* configurations of the NBD molecule occupy the same adsorption area corresponding to 4 fourfold sites. The NBD molecule directly occupies one fourfold site, and an area corresponding to 3 fourfold sites surrounds this molecule. In this regard, in contrast to the (111) surface, the *exo*-adsorption of NBD on the Pd(100) surface seems unlikely.

Multiple adsorption of NBD and NBE on Pd surface

In order to elucidate the possible effect of the environment of neighboring adsorbed NBD molecules on the adsorption energy, calculations for 2 to 4 adsorbed NBD molecules on the Pd surface were made (Figure S4). Figure 9 shows the dependence of the average adsorption energy (per one

Fig. 8 Estimation of adsorption area of one NBD molecule for the *endo-tetra-σ* (a) and *exo-di-σ* (b) configurations on (111) facet of Pd₈₆. Distances (Å) between the purple dots are shown



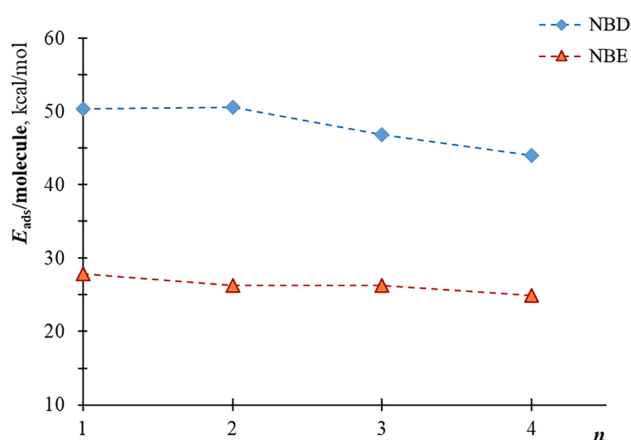


Fig. 9 Dependence of the average adsorption energy (E_{ads} /molecule) on the number (n) of the adsorbed NBD and NBE molecules on Pd(100)

molecule) on the number of the *endo-tetra- σ* adsorbed NBD and *exo-di- σ* adsorbed NBE molecules on Pd(100). It follows that the average adsorption energy of NBD decreases by about ~ 6 kcal/mol, while for NBE this value is lower (~ 3 kcal/mol). Thus, the repulsion between *endo*-adsorbed NBD molecules is stronger. Another factor in favor of the *exo*-adsorption of the NBD molecule on Pd(111).

Interconversion and migration of adsorption configurations on Pd surface

Another important aspect of surface chemistry concerns the interconversion and mobility of adsorption configurations on the Pd surface. According to our calculations, the *endo-di- π* adsorbed NBD molecule transforms into

a *di- σ,π* configuration with the very low (~ 0.5 kcal/mol) activation barrier. Then, with the same barrier, the *di- σ,π* configuration passes into the energetically more favorable *tetra- σ* configuration. Figure 10 shows a graph of the energy change along the reaction coordinate (C–Pd distance). The approach of the C3 atom of the *di- σ,π* configuration to the Pd1 atom leads to the formation of the *tetra- σ _1* configuration. The *tetra- σ _2* configuration is formed if the movement of the C2 atom of the *di- σ,π* configuration is directed to the Pd5 atom. It turns out that the *di- σ,π* configuration is an intermediate in the two-stage transformation of *tetra- σ _1* to *tetra- σ _2* with the low activation barriers (6.1–6.7 kcal/mol). Therefore, the *di- π* and *di- σ,π* configurations are not stable despite the high adsorption energy (25.9 and 37.8 kcal/mol, Table 3).

However, the *di- σ,π* configuration plays an important role as an intermediate in the migration of the NBD molecule. In contrast to the (111) facet, π -adsorption of double bonds of the *endo*-adsorbed NBD molecule on the (100) facet is impossible and, accordingly, the *di- σ,π* configuration is not formed. This leads to significant difficulties in the migration of the NBD molecule on Pd(100). According to our calculations, the activation barrier to migration of the NBD molecule is ~ 28 kcal/mol (Figure S5).

The configurations of the *exo*-adsorbed NBE molecule are also capable of interconversions on the (111) face. Thus, the π configuration easily transforms into a more energetically favorable *di- σ* configuration with the activation barrier of ~ 1 kcal/mol. Figure 11 shows the energy change in during the transition from one *di- σ* configuration to the same one through the intermediate formation of the π configuration. The activation barriers of the two-stage migration of the NBE molecule from the Pd1 and

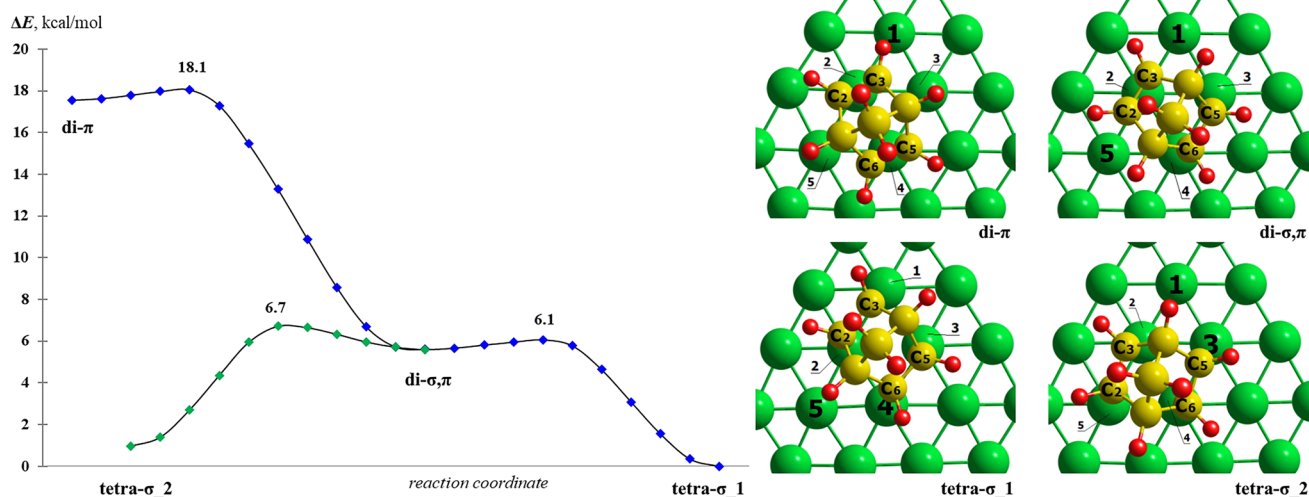


Fig. 10 Energy profile of interconversions of *di- π* , *di- σ,π* and *tetra- σ* configurations of the *endo*-adsorbed NBD molecule on Pd(111). The energies are given with respect to the *tetra- σ _1* configuration. The corresponding structures are shown on the right (top view of NBD)

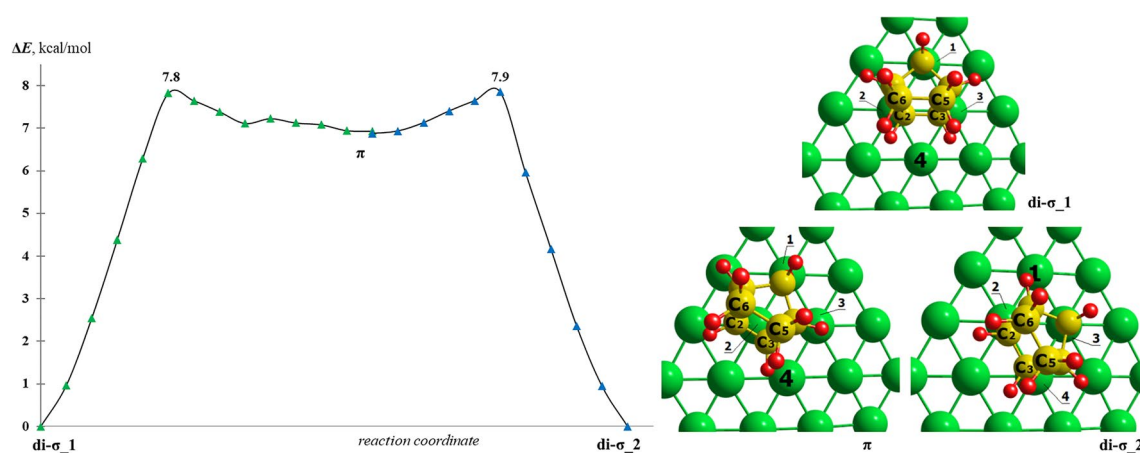


Fig. 11 Energy profile of interconversions of **di-σ** and π configurations of the *exo*-adsorbed NBE molecule on Pd(111). The energies are given with respect to the **di-σ**₁ configuration. The corresponding structures are shown on the right (top view of NBE)

Pd2 atoms (**di-σ**₁, Fig. 11) to the Pd2 and Pd3 atoms (**di-σ**₂, Fig. 11) do not exceed 8 kcal/mol. The transition from **di-σ**₁ to **di-σ**₂ is possible in one stage without intermediate formation of the π configuration. For example, the approach of the C2 atom to the Pd3 atom leads to the **di-σ**₂ configuration, but the activation barrier in this case is higher (~10 kcal/mol, Figure S6).

Migration of the *exo*-adsorbed NBE molecule is also possible on the (100) facet. The activation barrier of $\pi \rightarrow$ **di-σ** transformation is ~0.5 kcal/mol (Figure S7). Therefore, the transformation of one **di-σ** configuration into another **di-σ** through the intermediate formation of the π configuration will proceed with the activation barrier:

$$E^\ddagger = E_{\text{ads}}(\text{di-}\sigma) - E_{\text{ads}}(\pi) + E^\ddagger(\pi \rightarrow \text{di-}\sigma) = 5.1 \text{ kcal/mol}$$

Conclusions

In summary, the interaction of norbornadiene (NBD) and norbornene (NBE) molecules with the Pd(111) and Pd(100) surfaces have been investigated using the density functional theory (DFT-PBE) calculations. Five configurations of adsorbed NBD may be formed on Pd(111): *endo-tetra-σ*, *endo-di-σ,π*, *endo-di-π*, *exo-di-σ* and *exo-π*. The most energetically stable configuration is the *endo-tetra-σ* configuration with the adsorption energy of 43.7 kcal/mol. The NBE molecule adsorbed on Pd(111) may exist in 4 configurations: *endo-di-σ*, *endo-π*, *exo-di-σ* and *exo-π*. The most preferred is the *exo-di-σ* configuration ($E_{\text{ads}} = 25.8$ kcal/mol).

On the Pd(100) surface, a smaller number adsorption configurations of NBD and NBE are formed, since the double bonds of these molecules in the *endo*-orientation

are bound only in a *di-σ* configuration. Therefore, 3 NBD adsorption configurations (*endo-tetra-σ*, *exo-di-σ* and *exo-π*) and 3 NBE adsorption configurations (*endo-di-σ*, *exo-di-σ* and *exo-π*) are formed on Pd(100). The most stable adsorption configurations are *endo-tetra-σ* (NBD) and *exo-di-σ* (NBE) with the adsorption energies are 48.4 and 27.3 kcal/mol, respectively. Therefore, the adsorption of NBD and NBE on Pd(100) was found to be on about 2–5 kcal/mol stronger as compared to Pd (111).

Thus, on both clean Pd surfaces, the *endo*-adsorption with the formation of the *tetra-σ* configuration is preferred for NBD, while the NBE molecule is adsorbed in the *exo-di-σ* configuration. However, the possibility of NBD adsorption in the *exo-di-σ* configuration on Pd(111) cannot be ruled out. Due to smaller adsorption area of the *exo-di-σ* configuration on Pd(111), a larger number of NBD molecules may adsorbed on the surface. In addition, repulsion between *endo*-adsorbed NBD molecules is stronger.

In the *exo-di-σ* and *exo-π* configurations of NBD and NBE, the hydrogen atom of the CH₂-bridge group interacts with the Pd atoms. Geometric parameters (bond length H–Pd is 2.11–2.18 Å, $\angle\text{CHPd} = 156\text{--}171^\circ$) make it possible to classify this H–Pd interaction as anagostic, and the interaction energy is approximately equal to 6.4–7.7 kcal/mol.

The most energetically favorable *endo-tetra-σ* (NBD) and *exo-di-σ* (NBE) configurations are highly mobile on Pd(111) and their migration occurs with the low activation barriers (~6–8 kcal/mol). Migration of NBD on the (111) facet proceeds through the intermediate **di-σ,π** configurations, and NBE migrates through the π configurations. On Pd(100), only NBE molecules with the activation barriers of ~5 kcal/mol can migrate, while NBD migration is hindered due to the high activation barriers (~28 kcal/mol).

Supplementary Information The online version contains supplementary material available at <https://doi.org/10.1007/s00894-023-05738-7>.

Acknowledgements The Author would like to thank Artem Shamsiev for his help in translating this paper. Calculations were carried out on computational facilities at the Joint Supercomputer Center of the Russian Academy of Sciences.

Author contributions Study conception, modeling, calculations, analysis, and manuscript preparation.

Funding The work was financially supported by the Russian Science Foundation (Project No. 23–73–00123).

Data availability The data used to support the findings of this study are available from the corresponding author upon request.

Declarations

Competing interests The authors declare no competing interests.

References

- Dzhemilev UM, Khusnutdinov RI, Tolstikov GA (1987) Norbornadienes in the Synthesis of Polycyclic Strained Hydrocarbons with Participation of Metal Complex Catalysts. *Russ Chem Rev* 56:36–51. <https://doi.org/10.1070/RC1987v056n01ABEH003255>
- Durakov SA, Kolobov AA, Flid VR (2022) Features of heterogeneous catalytic transformations of strained carbocyclic compounds of the norbornene series. *Fine Chem Technol* 17(4):275–297. <https://doi.org/10.32362/2410-6593-2022-17-4-275-297>
- Finkelshtein ESh, Bermeshev MV, Gringolts ML, Starannikova LE, Yampolskii YuP (2011) Substituted polynorbornenes as promising materials for gas separation membranes. *Russ Chem Rev* 80:341–362. <https://doi.org/10.1070/RC2011v080n04ABEH004203>
- Yalçinkaya EE, Balcan M, Güler Ç (2013) Synthesis, characterization and dielectric properties of polynorbornadiene – clay nanocomposites by ROMP using intercalated Ruthenium catalyst. *Mater Chem Phys* 143:380–386. <https://doi.org/10.1016/j.matchemphys.2013.09.014>
- Ono Y, Kawashima N, Kudo H, Nishikubo T, Naga T (2005) Synthesis of new photoresponsive polyesters containing norbornadiene moieties by the ring-opening copolymerization of donor–acceptor norbornadiene dicarboxylic acid anhydride with donor–acceptor norbornadiene dicarboxylic acid monoglycidyl ester derivatives. *J Polym Sci Polym Chem* 43:4412–4421. <https://doi.org/10.1016/10.1002/pola.20911>
- Tsubata A, Uchiyama T, Kameyama A, Nishikubo T (1997) Synthesis of Poly(esteramide)s Containing Norbornadiene (NBD) Residues by the Polyaddition of NBD Dicarboxylic Acid Derivatives with Bis(epoxide)s and Their Photochemical Properties. *Macromolecules* 30:5649–5654. <https://doi.org/10.1021/ma970431a>
- Alentiev DA, Nikiforov RYu, Rudakova MA, Zarezin DP, Topchii MA, Asachenko AF, Alentiev AYu, Bolshchikov BD, Belov NA, Finkelshtein ESh, Bermeshev MV (2022) Polynorbornenes bearing ether fragments in substituents: Promising membrane materials with enhanced CO₂ permeability. *J Membrane Sci* 648:120340. <https://doi.org/10.1016/j.memsci.2022.120340>
- Bermeshev MV, Chapala PP (2018) Addition polymerization of functionalized norbornenes as a powerful tool for assembling molecular moieties of new polymers with versatile properties. *Prog Polym Sci* 84:1–46. <https://doi.org/10.1016/j.progpolymsci.2018.06.003>
- Fiorino F, Perissutti E, Severino B, Santagada V, Cirillo D, Terraciano S, Massarelli P, Bruni G, Collavoli E, Renner C, Caliendo G (2005) New 5-Hydroxytryptamine 1A Receptor Ligands Containing a Norbornene Nucleus: Synthesis and in Vitro Pharmacological Evaluation. *J Med Chem* 48:5495–5503. <https://doi.org/10.1021/jm050246k>
- Hajiyeva GE (2021) Biologically Active Norbornene Derivatives: Synthesis of Bicyclo[2.2.1]heptene Mannich Bases. *Chem Sustain Dev* 29(4):391–410. <https://doi.org/10.15372/CSD2021317>
- Carroll FI, Brieady LE, Navarro HA, Damaj MI, Martin BR (2005) Synthesis and Pharmacological Characterization of exo-2-(2'-Chloro-5-pyridinyl)-7-(endo and exo)-aminobicyclo[2.2.1]heptanes as Novel Epibatidine Analogues. *J Med Chem* 48:7491–7495. <https://doi.org/10.1021/jm058243v>
- Calvo-Martín G, Plano D, Martínez-Sáez N, Aydillo C, Moreno E, Espuelas S, Sanmartín C (2022) Norbornene and Related Structures as Scaffolds in the Search for New Cancer Treatments. *Pharmaceuticals* 15:1465. <https://doi.org/10.3390/ph15121465>
- Gusevskaya EV, Jiménez-Pinto J, Börner A (2014) Hydroformylation in the Realm of Scents. *ChemCatChem* 6:382–411. <https://doi.org/10.1002/cctc.201300474>
- Buchbauer G, Stappen I, Pretterklieber C, Wolschann P (2004) Structure–activity relationships of sandalwood odorants: synthesis and odor of tricyclo β-santalol. *Eur J Med Chem* 39:1039–1046. <https://doi.org/10.1016/j.ejmech.2004.09.014>
- Kudo H, Yamamoto M, Nishikubo T, Moriya O (2006) Novel Materials for Large Change in Refractive Index: Synthesis and Photochemical Reaction of the Ladderlike Poly(silsesquioxane) Containing Norbornadiene, Azobenzene, and Anthracene Groups in the Side Chains. *Macromolecules* 39:1759–1765. <https://doi.org/10.1021/ma052147m>
- Kato Y, Muta H, Takahashi S, Horie K, Nagai T (2001) Large Photoinduced Refractive Index Change of Polymer Films Containing and Bearing Norbornadiene Groups and Its Application to Submicron-Scale Refractive-Index Patterning. *Polym J* 33:868–873. <https://doi.org/10.1295/polymj.33.868>
- Dubonosov AD, Bren VA, Chernoiivanov VA (2002) Norbornadiene–quadricyclane as an abiotic system for the storage of solar energy. *Russ Chem Rev* 71:917–927. <https://doi.org/10.1070/RC2002v071n11ABEH000745>
- Gray V, Lennartson A, Ratanalert P, Börjessonab K, Moth-Poulsen K (2014) Diaryl-substituted norbornadienes with red-shifted absorption for molecular solar thermal energy storage. *Chem Commun* 50:5330–5332. <https://doi.org/10.1039/C3CC47517D>
- Mansø M, Petersen AU, Wang Z, Erhart P, Nielsen MB, Moth-Poulsen K (2018) Molecular solar thermal energy storage in photoswitch oligomers increases energy densities and storage times. *Nat Commun* 9:1945. <https://doi.org/10.1038/s41467-018-04230-8>
- Jevric M, Petersen AU, Mansø M, Singh SK, Wang Z, Dreos A, Sumbly C, Nielsen MB, Börjesson K, Erhart P, Moth-Poulsen K (2018) Norbornadiene-Based Photoswitches with Exceptional Combination of Solar Spectrum Match and Long-Term Energy Storage. *Chem Eur J* 24:12767–12772. <https://doi.org/10.1002/chem.201802932>
- Dreos A, Wang Z, Udmark J, Ström A, Erhart P, Börjesson K (2018) Liquid Norbornadiene Photoswitches for Solar Energy Storage. *Adv Energy Mater* 8:1703401. <https://doi.org/10.1002/aenm.201703401>
- Catellani M, Frignani F, Rangoni A (1997) A Complex Catalytic Cycle Leading to a Regioselective Synthesis of o, o'-Disubstituted Vinylarenes. *Angew Chem Int Ed Engl* 36:119–122. <https://doi.org/10.1002/anie.199701191>

23. Ye J, Lautens M (2015) Palladium-catalysed norbornene-mediated C-H functionalization of arenes. *Nature Chem* 7:863–870. <https://doi.org/10.1038/nchem.2372>
24. Wang J, Dong G (2019) Palladium/Norbornene Cooperative Catalysis. *Chem Rev* 119:7478–7528. <https://doi.org/10.1021/acs.chemrev.9b00079>
25. Khoury PR, Goddard JD, Tam W (2004) Ring strain energies: substituted rings, norbornanes, norbornenes and norbornadienes. *Tetrahedron* 60:8103–8112. <https://doi.org/10.1016/j.tet.2004.06.100>
26. Knuchel G, Grassi G, Vogelsanger B, Bauder A (1993) Molecular structure of norbornadiene as determined by microwave Fourier transform spectroscopy. *J Am Chem Soc* 115:10845–10848. <https://doi.org/10.1021/ja00076a047>
27. Brunelli M, Fitch AN, Jouanneaux A, Mora AJ (2001) Crystal and molecular structures of norbornene. *Zeitschrift für Kristallographie-Crystalline Mater* 216:51–55
28. Zamalyutin VV, Katsman EA, Danyushevsky VY, Flid VR, Podol'skii VV, Ryabov AV (2021) Specific Features of the Catalytic Hydrogenation of the Norbornadiene-Based Carbocyclic Compounds. *Russ J Coord Chem* 47:695–701. <https://doi.org/10.1134/S1070328421100080>
29. Borodziński A, Bond GC (2006) Selective Hydrogenation of Ethyne in Ethene-Rich Streams on Palladium Catalysts. Part 1. Effect of Changes to the Catalyst During Reaction. *Catal Rev* 48:91–144. <https://doi.org/10.1080/01614940500364909>
30. Rassolov AV, Bragina GO, Baeva GN, Mashkovsky IS, Stakheev AY (2020) Alumina-Supported Palladium-Silver Bimetallic Catalysts with Single-Atom Pd1 Sites in the Liquid-Phase Hydrogenation of Substituted Alkynes. *Kinet Catal* 61:869–878. <https://doi.org/10.1134/S0023158420060129>
31. Katano S, Kato HS, Kawai M, Domen K (2003) Selective Partial Hydrogenation of 1,3-Butadiene to Butene on Pd(110): Specification of Reactant Adsorption States and Product Stability. *J Phys Chem B* 107:3671–3674. <https://doi.org/10.1021/jp022410a>
32. Méndez FJ, Solano R, Villasana Y, Guerra J, Curbelo S, Inojosa M, Olivera-Fuentes C, Brito JL (2016) Selective hydrogenation of 1,3-butadiene in presence of 1-butene under liquid phase conditions with NiPd/Al₂O₃ catalysts. *Appl Petrochem Res* 6:379–387. <https://doi.org/10.1007/s13203-016-0149-y>
33. Schmidt A, Schomäcker R (2007) Kinetics of 1,5-Cyclooctadiene Hydrogenation on Pd/ α -Al₂O₃. *Ind Eng Chem Res* 46:1677–1681. <https://doi.org/10.1021/ie0611958>
34. Benaissa M, Alhanash AM, Eissa M, Hamdy MS (2017) Solvent-free selective hydrogenation of 1,5-cyclooctadiene catalyzed by palladium incorporated TUD-1. *Catal Commun* 101:62–65. <https://doi.org/10.1016/j.catcom.2017.07.026>
35. Zhao Z, Wang Y (2020) Thermoregulated Phase-Transfer Pd Nanocatalyst for Selective Hydrogenation of 1,5-Cyclooctadiene at Atmospheric Hydrogen Pressure. *Catal Lett* 150:2703–2708. <https://doi.org/10.1007/s10562-020-03174-3>
36. Krier JM, Komvopoulos K, Somorjai GA (2016) Cyclohexene and 1,4-Cyclohexadiene Hydrogenation Occur through Mutually Exclusive Intermediate Pathways on Platinum Nanoparticles. *J Phys Chem C* 120:8246–8250. <https://doi.org/10.1021/acs.jpcc.6b01615>
37. Qi S, Yu W, Lonergan WW, Yang B, Chen JG (2010) General Trends in the Partial and Complete Hydrogenation of 1,4-Cyclohexadiene over Pt–Co, Pt–Ni and Pt–Cu Bimetallic Catalysts. *ChemCatChem* 2:625–628. <https://doi.org/10.1002/cctc.201000082>
38. Zhao X, Chang Y, Chen W-J, Wu Q, Pan X, Chen K, Weng B (2022) Recent Progress in Pd-Based Nanocatalysts for Selective Hydrogenation. *ACS Omega* 7:17–31. <https://doi.org/10.1021/acsomega.1c06244>
39. Bauer U, Fromm L, Weiß C, Bachmann P, Späth F, Düll F, Steinhauer J, Hieringer W, Görling A, Hirsch A, Steinrück H-P, Papp C (2019) Controlled Catalytic Energy Release of the Norbornadiene/Quadracyclane Molecular Solar Thermal Energy Storage System on Ni(111). *J Phys Chem C* 123:7654–7664. <https://doi.org/10.1021/acs.jpcc.8b03746>
40. Hemauer F, Bauer U, Fromm L, Weiß C, Leng A, Bachmann P, Düll F, Steinhauer J, Schwaab V, Grzonka R, Hirsch A, Görling A, Steinrück H-P, Papp C (2022) Surface Chemistry of the Molecular Solar Thermal Energy Storage System 2,3-Dicyano-Norbornadiene/Quadracyclane on Ni(111). *ChemCatChem* 23:e202200199. <https://doi.org/10.1002/cphc.202200199>
41. Hostetler M, Nuzzo R, Girolami G, Dubois L (1995) Norbornadiene on Pt(111) Is Not Bound as an $\eta^2:\eta^2$ Diene: Characterization of an Unexpected $\eta^2:\eta^1$ Bonding Mode Involving an Agostic Pt–H–C Interaction. *Organometallics* 14:3377–3384. <https://doi.org/10.1021/om00007a044>
42. Bauer U, Mohr S, Döpfer T, Bachmann P, Späth F, Düll F, Schwarz M, Brummel O, Fromm L, Pinkert U, Görling A, Hirsch A, Bachmann J, Steinrück H-P, Libuda J, Papp C (2017) Catalytically Triggered Energy Release from Strained Organic Molecules: The Surface Chemistry of Quadracyclane and Norbornadiene on Pt(111). *Chem Eur J* 23:1613–1622. <https://doi.org/10.1002/chem.201604443>
43. Bilić A, Reimers JR, Hush NS (2003) Modeling the adsorption of norbornadiene on the Si(001) surface: The predominance of non-[2+2]-cycloaddition products. *J Chem Phys* 119:1115–1126. <https://doi.org/10.1063/1.1577539>
44. Kim A, Choi J, Kim DH, Kim S (2009) Structural Properties of Norbornene Monolayers on Ge(100). *J Phys Chem C* 113:14311–14315. <https://doi.org/10.1021/jp901360g>
45. Laikov DN (1997) Fast evaluation of density functional exchange-correlation terms using the expansion of the electron density in auxiliary basis sets. *Chem Phys Lett* 281:151–156. [https://doi.org/10.1016/S0009-2614\(97\)01206-2](https://doi.org/10.1016/S0009-2614(97)01206-2)
46. Laikov DN, Ustynyuk YuA (2005) PRIRODA-04: A quantum-chemical program suite. New possibilities in the study of molecular systems with the application of parallel computing. *Russ Chem Bull* 54:820–826. <https://doi.org/10.1007/s11172-005-0329-x>
47. Perdew JP, Burke K, Ernzerhof M (1996) Generalized Gradient Approximation Made Simple. *Phys Rev Lett* 77:3865–3868. <https://doi.org/10.1103/PhysRevLett.77.3865>
48. Stevens WJ, Basch H, Krauss M (1984) Compact effective potentials and efficient shared exponent basis sets for the first and second row atoms. *J Chem Phys* 81:6026–6033. <https://doi.org/10.1063/1.447604>
49. Shamsiev RS, Danilov FO (2017) Quantum chemical study of H₂ adsorption on Pd₂₁ cluster. *Russ Chem Bull* 66:395–400. <https://doi.org/10.1007/s11172-017-1746-3>
50. Laikov DN (2019) Atomic basis functions for molecular electronic structure calculations. *Theor Chem Acc* 138:40. <https://doi.org/10.1007/s00214-019-2432-3>
51. Laikov DN (2020) Optimization of atomic density-fitting basis functions for molecular two-electron integral approximations. *J Chem Phys* 153:114121. <https://doi.org/10.1063/5.0014639>
52. Adamo C, Barone V (1999) Toward reliable density functional methods without adjustable parameters: The PBE0 model. *J Chem Phys* 110:6158–6170. <https://doi.org/10.1063/1.478522>
53. Moskaleva LV, Chen Z-X, Aleksandrov HA, Mohammed AB, Sun Q, Rösch N (2009) Ethylene Conversion to Ethylidyne over Pd(111): Revisiting the Mechanism with First-Principles Calculations. *J Phys Chem C* 113:2512–2520. <https://doi.org/10.1021/jp8082562>
54. Chen Z-X, Aleksandrov HA, Basaran D, Rösch N (2010) Transformations of Ethylene on the Pd(111) Surface: A Density Functional Study. *J Phys Chem C* 114:17683–17692. <https://doi.org/10.1021/jp104949w>
55. Yang B, Burch R, Hardacre C, Headdock G, Hu P (2013) Influence of surface structures, subsurface carbon and hydrogen, and surface

- alloying on the activity and selectivity of acetylene hydrogenation on Pd surfaces: A density functional theory study. *J Catal* 305:264–276. <https://doi.org/10.1016/j.jcat.2013.05.027>
56. Shamsiev RS, Finkelshtein EI (2018) Adsorption of phenylacetylene and styrene on palladium surface: a DFT study. *J Mol Model* 24:143. <https://doi.org/10.1007/s00894-018-3685-9>
 57. Benet-Buchholz J, Haumann T, Boese R (1998) How to circumvent plastic phases: the single crystal X-ray analysis of norbornadiene. *Chem Commun* 18:2003–2004. <https://doi.org/10.1039/A804842H>
 58. Doms L, Van den Enden L, Geise HJ, Van Alsenoy C (1983) Structure determination of gaseous norbornane by electron diffraction, microwave, Raman, and infrared spectroscopy. Molecular mechanics and ab initio calculations with complete geometry relaxation. *J Am Chem Soc* 105:158–162. <https://doi.org/10.1021/ja00340a002>
 59. Mackenzie-Ross H, Brunger MJ, Wang F, Adcock W, Maddern T, Campbell L, Newell WR, McCarthy IE, Weigold E, Appelbe B, Winkler DA (2002) Comprehensive Experimental and Theoretical Study into the Complete Valence Electronic Structure of Norbornadiene. *J Phys Chem A* 106:9573–9581. <https://doi.org/10.1021/jp021338d>
 60. Brookhart M, Green MLH, Parkin G (2007) Agostic interactions in transition metal compounds. *Proc Natl Acad Sci* 104:6908–6914. <https://doi.org/10.1073/pnas.0610747104>
 61. Morin C, Simon D, Sautet P (2006) Intermediates in the hydrogenation of benzene to cyclohexene on Pt(111) and Pd(111): A comparison from DFT calculations. *Surf Sci* 600:1339–1350. <https://doi.org/10.1016/j.susc.2006.01.033>
 62. Lee TR, Whitesides GM (1992) Heterogeneous, platinum-catalyzed hydrogenations of (diolefin)dialkylplatinum(II) complexes. *Acc Chem Res* 25:266–272. <https://doi.org/10.1021/ar00018a004>
 63. Shamsiev RS, Danilov FO, Flid VR (2018) Quantum chemical analysis of mechanisms of phenylacetylene and styrene hydrogenation to ethylbenzene on the Pd{111} surface. *Russ Chem Bull* 67:419–424. <https://doi.org/10.1007/s11172-018-2088-5>
 64. Shamsiev RS, Danilov FO (2018) DFT Modeling of mechanism of hydrogenation of phenylacetylene into styrene on a Pd(111) surface. *Kinet Catal* 59:333–338. <https://doi.org/10.1134/S0023158418030187>

Publisher's Note Springer Nature remains neutral with regard to jurisdictional claims in published maps and institutional affiliations.

Springer Nature or its licensor (e.g. a society or other partner) holds exclusive rights to this article under a publishing agreement with the author(s) or other rightsholder(s); author self-archiving of the accepted manuscript version of this article is solely governed by the terms of such publishing agreement and applicable law.